Available online at www.sciencedirect.com
ScienceDirect
Trans. Nonferrous Met. Soc. China 30(2020) 1−13
Transactions of Nonferrous Metals Society of China
www.tnmsc.cn

Effect of melt holding on morphological evolution and sedimentation behavior of iron-rich intermetallic phases in Al−Si−Fe−Mn−Mg alloy

Dong-fu SONG[1,2], Shun-cheng WANG[2], Yu-liang ZHAO[3], Shu-hong LIU[4], Yong DU[4], Yue-hua KANG[2], Zhi WANG[1], Wei-wen ZHANG[1]

1. National Engineering Research Centre of Near-net-shape Forming for Metallic Materials, South China University of Technology, Guangzhou 510641, China;
2. Guangdong Institute of Materials and Processing, Guangzhou 510650, China;
3. School of Mechanical Engineering, Dongguan University of Technology, Dongguan 523808, China;
4. State Key Laboratory of Powder Metallurgy, Central South University, Changsha 410083, China

Received 10 April 2019; accepted 11 November 2019

Abstract: The effect of the melt holding temperature on the morphological evolution and sedimentation behavior of iron-rich intermetallics in Al−7.0Si−1.0Fe−1.2Mn−0.25Mg alloy was investigated using an optical microscope, scanning electron microscope and differential thermal analyzer. The results show that as the holding temperature decreases, the morphologies of the primary iron-rich phase in matrix change from star-like to polygonal, and the number of the primary phases gradually decreases and disappears at 615 °C. Finally, the Chinese script phases with small size, high compact and uniform distribution are obtained. In contrast, the primary iron-rich phases in slag transform into a coarser polygonal shape with lower roundness, and some of them have hollow structures. Furthermore, the area fraction of intermetallics and Fe content in the matrix decrease gradually due to the formation and growth of sludge and subsequent natural sedimentation during melt holding. With the decrease of holding temperature, the main factors hindering the settlement of the primary phases are morphology, size, and density in turn.

Key words: Al−Si alloy; melt holding; iron-rich intermetallic phases; morphological evolution; sedimentation behaviour

1 Introduction

Iron (Fe) is one of the common impurity elements of Al−Si system alloys. Since it forms iron-rich intermetallics with high brittleness and hardness, Fe is usually considered a harmful element; specially the long and narrow needle-like iron-rich phase (β-Al_5FeSi phase) is especially significantly deleterious to the plasticity because of the serious separation of the Al matrix [1,2]. In contrast, another type of iron-rich intermetallic phase (α-Al_8Fe_2Si phase) with a Chinese script morphology results in less separation due to its smaller size and higher density. Furthermore, α-Al_8Fe_2Si intermetallics might be used as beneficial phases to improve the strength and wear resistance [3,4]. Therefore, improving the morphology of the iron-rich phase has become an effective method for relieving the harm caused by Fe impurities.

Foundation item: Project (2017GDASCX-0117) supported by the Guangdong Academy of Sciences, China; Project (201806010126) supported by the Pearl River S&T Nova Program of Guangzhou, China; Projects (2017A050503004, 2017A07071029) supported by the Guangdong Provincial Program of Science and Technology, China; Project (18126010) supported by the Guangxi Autonomous Regional Program of Science and Technology, China; Project (201802030012) supported by the Guangzhou Municipal Science and Technology Bureau, China; Project(2017A0109005) supported by the Sihui Plan Project of Science and Technology, China

Corresponding author: Wei-wen ZHANG; Tel: +86-20-87112022; E-mail: mewzhang@scut.edu.cn

DOI: 10.1016/S1003-6326(19)65175-7

At present, the methods for transforming the iron-rich phase morphology can be classified into two types, namely, element neutralization and optimized smelting and casting. The former involves adding elements such as Mn, Cr, Be, Sr, B, Sc and rare earth elements [5−10]. Subsequently, the morphology transforms from noodle-like to a smaller size and more compact structure through modifying the crystal structure, solidification sequence or growth speed of the iron-rich phases. The latter includes melt treatment, promotion of the cooling rate and use of the special casting methods [11−13]. These methods can be used to refine the size of intermetallics by eliminating or utilizing their inherent effects, physically breaking them or inhibiting their growth in space and time.

The addition of Mn is the most common method for reducing detrimental phases, as Mn can replace Fe atoms and transform the crystal structure from monoclinic tetragonal (β-Al_5FeSi) to simple cubic or body-centered cubic (α-Al_8Fe_2Si). Although its modification mechanism and improvement effects have been recognized by many researchers [5,11,14,15], the optimal amount of Mn addition is still not well established because the neutralization effects are deeply influenced by many factors, such as the cooling rate, melt treatment, initial Si and Fe contents, and other elements. When the Mn/Fe mole ratio is too small, the β-Al_5FeSi phase cannot be completely eliminated [16], whereas when the Mn/Fe mole ratio is too high, a primary phase (sludge) with a coarse size and a high density easily forms; this phase is harmful to the mechanical properties as well as the surface quality and machining difficulty [1,4]. However, these phases can be removed through electromagnetic separation, ceramic filtration or gravity sedimentation [17−19]. To reduce the Mn amount for neutralization and improve the Fe removal efficiency, many scholars have employed the addition of Mn combined with melt holding. ZHANG et al [20] found that holding at a high temperature before casting was beneficial to reducing the Mn content required to eliminate the β-Al_5FeSi phase. WANG et al [21] indicated that cooling the melt temperature to 610−620 °C in a furnace after holding at 850 °C can effectively promote transformation of the β-Al_5FeSi phase into α-Al_8Fe_2Si and improve the sedimentation efficiency of iron-bearing phases. LOPES et al [17] reported that more than 80% of the Fe content of Al−Si−Fe−Mn alloy was removed by holding at 605−645 °C for 30 min and then applying ceramic filtration. CAO and CAMPBELL [22] combined adding Mn with a holding treatment at low temperature for an Al−Si alloy with a high Fe content, and the removal ratio of Fe could reach more than 70% when n(Mn)/n(Fe)>1. Therefore, using Mn addition and a melt treatment together not only promotes beneficial transformation of iron-rich phases but also leads to the formation of a large amount of coarse, regular and high-density sludge, thus providing the necessary conditions for subsequent ceramic filtration and natural sedimentation for Fe removal. However, the previous research mainly focused on the sedimentation efficiency, its influencing factors and a simple description of the phenomenon; the morphology evolution and sedimentation control factors of sludge during the holding process have not been discussed in detail. This investigation focused on the effects of the melt holding temperature on the Fe content and morphologies of iron-rich phases to reveal the evolution mechanism and the natural sedimentation behavior of the iron-rich phase.

2 Experimental

The experimental alloys were prepared from commercial A356 alloy, A1−20Fe and Al−10Mn master alloys inside a graphite crucible resistance furnace. An A356 alloy ingot with 1.0% Fe was first prepared and divided into five equal parts, which were remelted at 800 °C with the addition of the required amount of Al−10Mn and then dropped to certain temperatures in the furnace and held for 1 h. Subsequently, the melt was poured into a 250 °C pretreated steel mold (200 mm × 30 mm × 150 mm), and the slag that remained in the furnace bottom was collected.

The chemical compositions of each alloy were determined via optical emission spectroscopy (SPECTRO-MAX), and the results are listed in Table 1. For the microstructure investigation and property tests, all the specimens were taken from the bottom of the ingot and prepared using a line-cutting machine. The sample dimensions and method of tensile testing followed GB/T 228.1−2010 and performed with a strain rate of 2 mm/min

Table 1 Chemical compositions of alloys after melt holding (wt.%)

Alloy No.	*T*/°C	Si	Fe	Mn	Mg	Al
1	680	7.05	0.92	1.17	0.25	Bal.
2	660	6.91	0.83	1.01	0.28	Bal.
3	645	6.92	0.64	0.82	0.20	Bal.
4	630	6.97	0.55	0.65	0.22	Bal.
5	615	7.03	0.43	0.42	0.21	Bal.

at room temperature. The data reported below are averages of at least three effective samples. The metallographic samples, including matrix alloy, slag and fracture section, were encased in epoxy resin, ground with SiC-based emery paper and polished by a diamond suspension. The microstructures were observed via optical microscopy (OM, Leica DM IRM) after etching with 0.5% HF solution for 15−60 s. The morphologies and compositions of phases were analyzed using scanning electron microscopy (SEM, JEOL JXA−8100) and energy dispersive spectroscopy (EDS, OXFORD−7412). The morphological characteristics of iron-rich intermetallics, including the equivalent diameter, roundness and area fraction, were analyzed using the Image-Pro Plus software package. To obtain relatively accurate data, approximately 30 different regions of each sample were measured at a magnification of 500 times. The solidification behavior of matrix alloys was studied using differential scanning calorimetry (DSC, STA409PC), and the phase compositions were tested via X-ray diffraction (XRD, Smartlab 9kW X). To analyze the evolution of the equilibrium phase, the isothermal section of the melt at different temperatures was calculated using thermo-calculation software based on an Al−Si−Fe−Mn thermodynamic database [23].

3 Results

3.1 Iron removal ratio

Table 1 lists the mass fraction of Fe and Mn elements in the alloys 1−5 after melt holding. The data indicate that the Fe and Mn contents were gradually reduced as the holding temperature decreased. When the holding temperature (HT, *T*) was 615 °C, the contents of Fe and Mn in the matrix were 0.43% and 0.42%, respectively, which were 53.3% and 64.1% lower than those at 680 °C.

3.2 Microstructure

Figure 1 shows the optical images of alloys 1−5 after melt holding. When the melt temperature was 680 °C, the iron-rich phase presented an irregular distribution, and an obvious difference was observed between the matrix grain types within the iron-rich and iron-poor areas, which corresponded to equiaxed grains and branched *α*(Al) dendrites, respectively. With a further decrease in the holding temperature, the amount of iron-rich phase was gradually reduced, and the

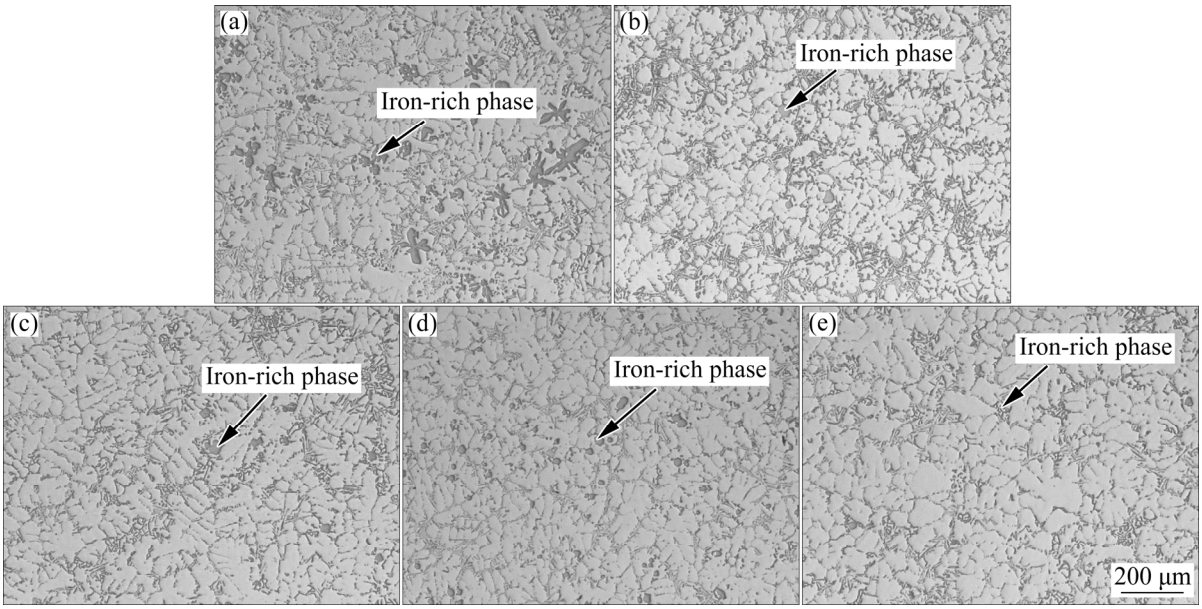

Fig. 1 Optical images of alloys after holding at different temperatures: (a) 680 °C, alloy 1; (b) 660 °C, alloy 2; (c) 645 °C, alloy 3; (d) 630 °C, alloy 4; (e) 615 °C, alloy 5

distribution uniformity was improved. The morphological distribution uniformity of alloys 4 and 5 was substantially improved compared to alloy 1, not only for the iron-rich intermetallics but also for the α(Al) dendrites. Meanwhile, the amount and size of iron-rich phases were further reduced, and α(Al) dendrites basically disappeared; instead, equiaxed grains with large areas were observed. Especially at 615 °C, the slag phase almost disappeared, whereas the matrix grains grew slightly.

Figure 2 shows the optical images of a typical iron-rich phase after holding at different temperatures. After holding at 680 °C, the coarse and star-like primary phase and a slender Chinese script phase were found in the matrix. The length of the sludge phase was more than 60 μm, and some sludge regions exceeded 100 μm. When the holding temperature was decreased to 645−660 °C, the sludge morphology transformed to a comparatively regular polygon connected to Chinese script. Upon further decreasing the holding temperature to 630 °C, the morphology of the primary iron-rich phase was similar to that at 660 °C, but the size was much smaller, and some of the Chinese script phase presented granular and short rods, which were more compact than those observed at higher holding temperatures. When the holding temperature was further decreased to 615 °C, the sludge phase basically disappeared, and only the Chinese script phase with a small size, high compaction and uniformity remained in the matrix. Therefore, with decreasing holding temperature, the morphology evolution sequence of the iron-rich phase can be summarized as follows: star-like + slender Chinese script → comparatively regular polygonal + slender Chinese script → small and regular polygonal + compact Chinese script → compact Chinese script.

To explore the reasons for the decrease in the area fraction of the iron-rich phase, SEM images of slag settled at the furnace bottom were obtained, as shown in Fig. 3. When the holding temperature was 630 °C, all of the iron-rich phases transformed into sludge phases with a regular and polygonal shape, as well as a uniform size and distribution, which were more compact than all the types of sludge phases observed in the matrix. As the holding temperature decreased, the sludge size became larger, and the morphology transformed into irregular polygons with hollow rhombi, which resulted in a low roundness and a relative decrease in the density. The formation mechanism of hollow rhombic sludge has already been reported in Ref. [24].

Figure 4 shows the statistical data of iron-rich phases after melt holding. The area fraction of intermetallics increased gradually as the holding temperature increased. When the holding temperature was 615 °C, the area fraction of the iron-rich phase was approximately 1.84%, which was only 50.4% of that holding at 680 °C. As shown in Fig. 4(b), no obvious regularity was found

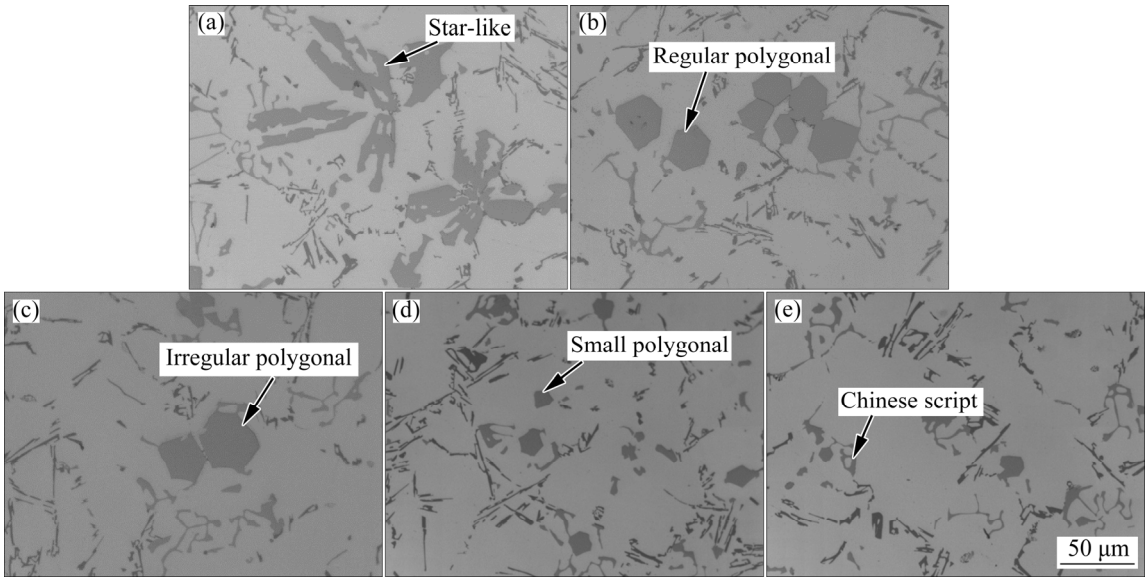

Fig. 2 Optical images of iron-rich phase in matrix holding at 680 °C (a), 660 °C (b), 645 °C (c), 630 °C (d) and 615 °C (e)

regarding the particle size, roundness and holding temperature. The roundness R_a used for characterizing the shape factor of sludge can be calculated using the following formula:

$$R_a=P^2/4\pi A \quad (1)$$

where P and A represent the perimeter and area of the sludge phase, respectively. According to the formula, the roundness of a standard circle is 1; when a shape is closer to a circle, the roundness is closer to 1. Figure 5 shows the roundness values of the typical primary phase, which indicates that the roundness is mainly determined by the morphology, and the roundness value sequence from large to small is star-like, irregular polygonal and regular polygonal.

Table 2 presents the morphological data of the iron-rich phase in slag. Compared with the matrix at 630 °C, the area fraction and size of the iron-rich phase in slag were significantly increased by 11.2 and 3.3 times, respectively. In addition, as the holding temperature decreased, the area fraction and size of primary phase increased sharply, while the shape factor slightly decreased.

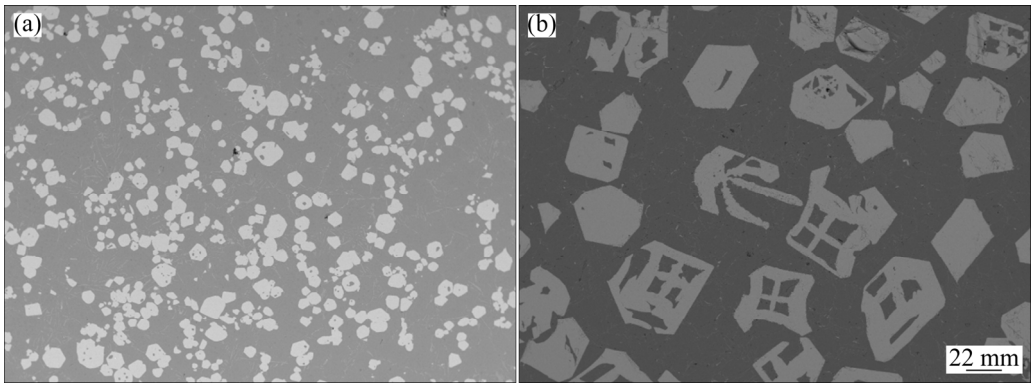

Fig. 3 SEM images of iron-rich intermetallics in slag at different holding temperatures: (a) 630 °C; (b) 615 °C

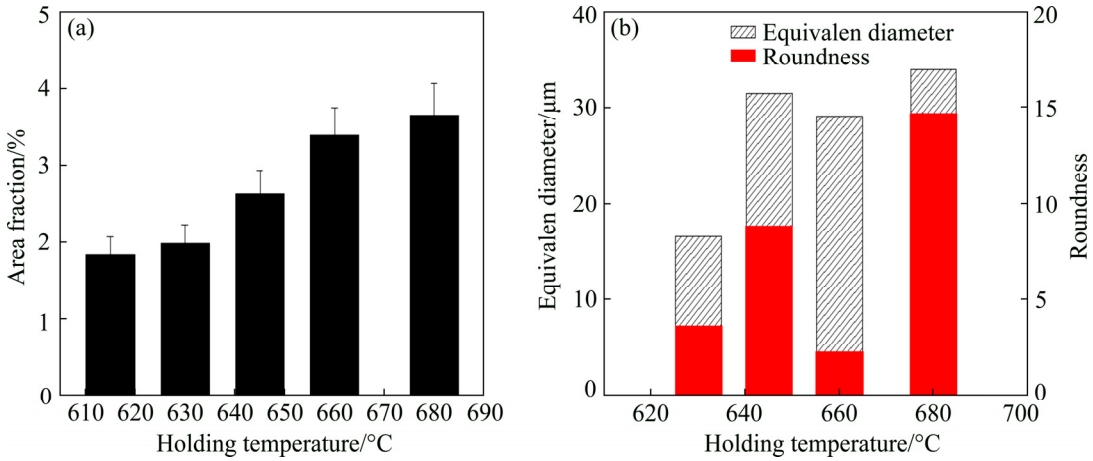

Fig. 4 Morphology characteristics of iron-rich intermetallics: (a) Area fraction of iron-rich intermetallics; (b) Equivalent diameter and roundness of sludge

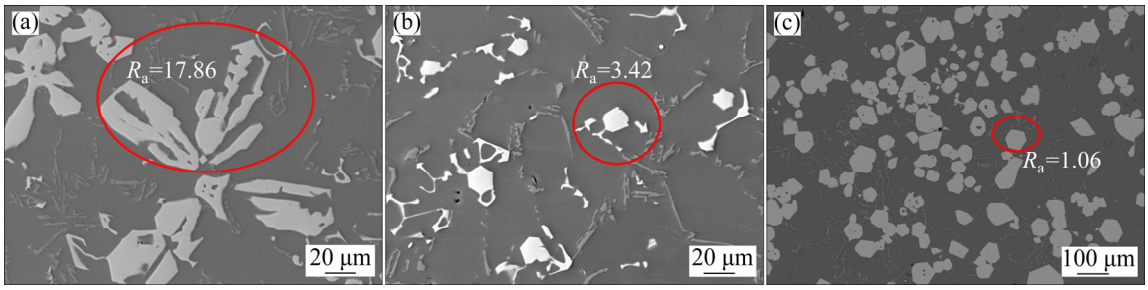

Fig. 5 Roundness of sludge with different morphologies: (a) Star-like; (b) Irregular polygonal; (c) Regular polygonal

Table 2 Morphological statistical data of iron-rich phase in slag

T/°C	Area fraction/%	Equivalent diameter/μm	Roundness
630	22.3±1.1	55±2	1.16±0.2
615	25.8±1.3	120±5	1.25±0.4

3.3 Chemical composition

The chemical composition of the iron-rich phase is reported in Table 3. As can be analyzed from the data, the (MnFe)/Si mole ratio of sludge was approximately 2.0±0.10, whether in the slag or matrix, and had no relation with the morphology or location. In contrast, the Mn/Fe mole ratio exhibited an obvious difference between the sludge and matrix, and the Mn/Fe mole ratio was stabilized at 1.7±0.02 in the slag, which was much higher than that in the matrix except for in alloy 4. The (MnFe)/Si and Mn/Fe mole ratios of the Chinese script phase were less than those of the sludge phase. WANG et al [21] measured the density of Al−Si−Mn−Fe iron-rich intermetallics with different Mn contents using the Archimedes method. The iron-rich intermetallic density reached 3.5−4.0 g/cm^3 with higher Mn contents, and the density of the phase increased gradually with increasing Mn content. Although the density and morphology of the primary iron-rich phase formed at 660 °C fixed in the matrix were similar to those in slag, the roundness was slightly lower than that in slag due to the growth of some whiskers on the edges of the polygons. To reveal the stage of whisker formation, the liner scanning spectrum of chemical composition of sludge phase in matrix holding at 660 °C was examined, as shown in Fig. 6. From the test results, the Mn content in the whisker and sludge edges was 18.9% lower than that in the central area, while the Fe content was 10.3% higher than that in the center. Therefore, the iron-rich phase located at the sludge edges can be inferred to form during the pouring stage of casting, not during the melt holding period.

3.4 Thermal analysis

Differential thermal analysis was performed on alloys 1 and 5 at a heating and cooling rate of 2 °C/min, and the corresponding DSC cooling curves are given in Fig. 7. The curve of alloy 1 exhibits a peak corresponding to the sludge phase up to 646.7 °C, and its initial formation temperature was approximately 661.4 °C, as calculated via thermal analysis, which is basically consistent with the temperature from the equation: Temperature= 645.7+34.2w^2(Fe) found in Ref. [6]. Meanwhile, the peak of the Chinese script phase was also detected at 610.7 °C, slightly higher than the temperature of the α(Al) phase (606.4 °C). After holding at 615 °C, the peak corresponding to the Chinese script phase was not found since it merged with the α(Al) phase peak, as shown in the cooling curve of alloy 5. The amount of iron-rich phase residing in the matrix 5 was greatly reduced after melt holding at 615 °C.

3.5 Phase analysis

Figure 8 shows the XRD curves of the matrix

Table 3 Chemical compositions of iron-rich intermetallics after holding (wt.%)

T/°C	Morphology	Al	Si	Mn	Fe	*n*(MnFe)/*n*(Si)	*n*(Mn)/*n*(Fe)
680	Star-like	55.78	8.82	20.89	14.50	2.01	1.44
	Chinese script	55.69	9.39	18.56	16.36	1.86	1.13
660	Polygonal	56.03	8.76	22.16	13.05	2.01	1.70
	Chinese script	59.41	9.07	17.04	14.39	1.74	1.19
645	Polygonal	56.54	8.54	20.60	14.32	2.04	1.44
	Chinese script	59.26	9.31	16.95	14.48	1.69	1.17
630	Polygonal	54.93	8.98	20.33	15.76	2.01	1.29
	Chinese script	54.50	9.73	16.70	19.08	1.84	0.88
	Sludge	57.50	8.28	21.59	12.64	2.07	1.71
615	Chinese script	73.81	6.73	9.63	9.83	1.44	0.98
	$\text{Sludge}_{615°C}$	57.81	8.68	21.30	12.41	1.94	1.72

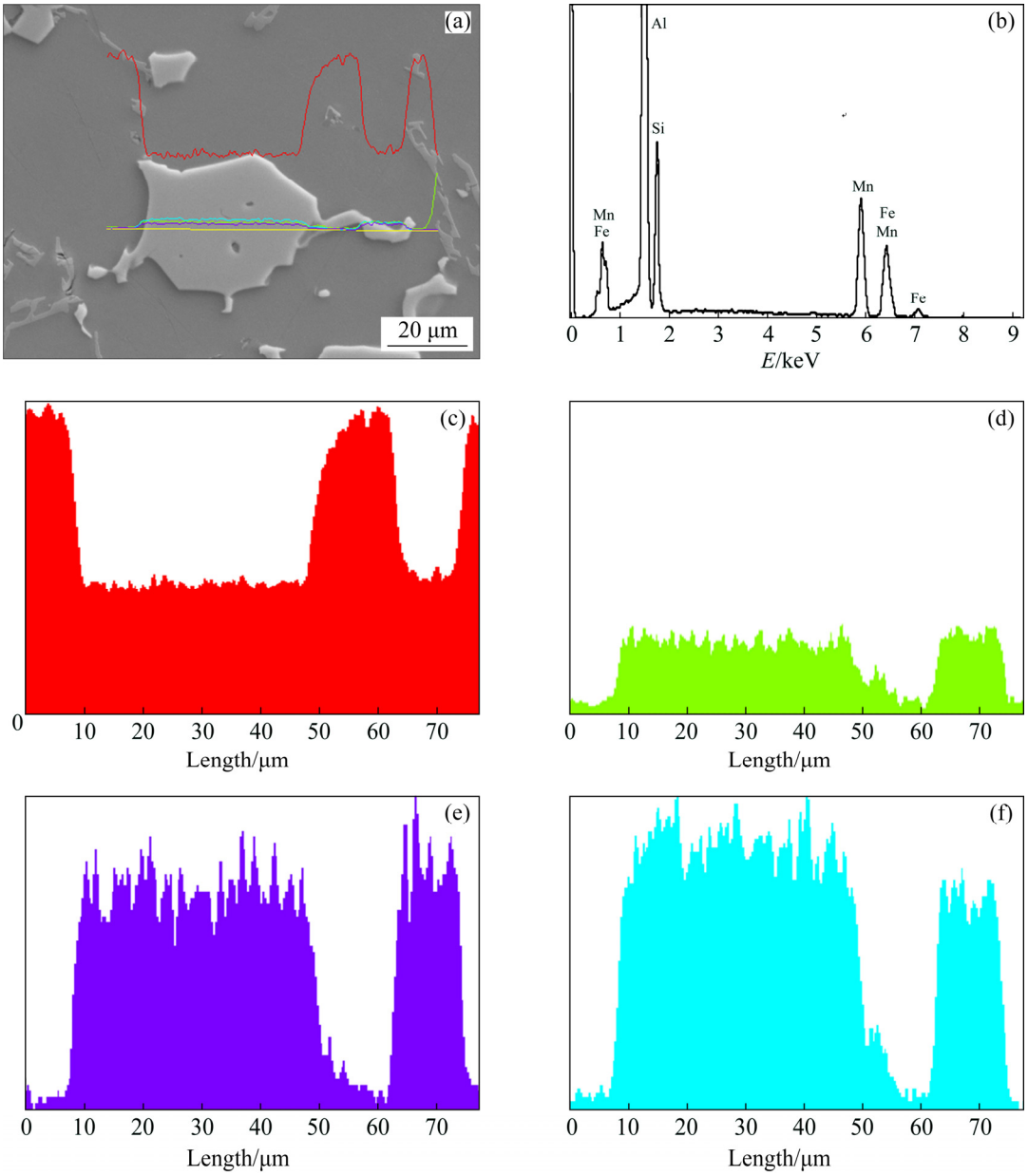

Fig. 6 Element distribution of sludge phase in matrix holding at 660 °C: (a) SEM image; (b) EDS pattern; (c) Al; (d) Si; (e) Fe; (f) Mn

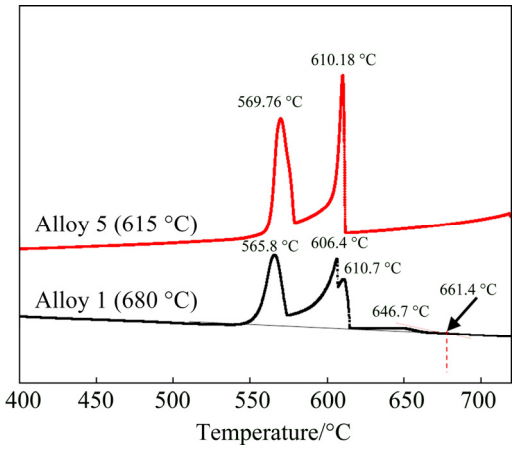

Fig. 7 DSC curves of matrix holding at 680 and 615 °C

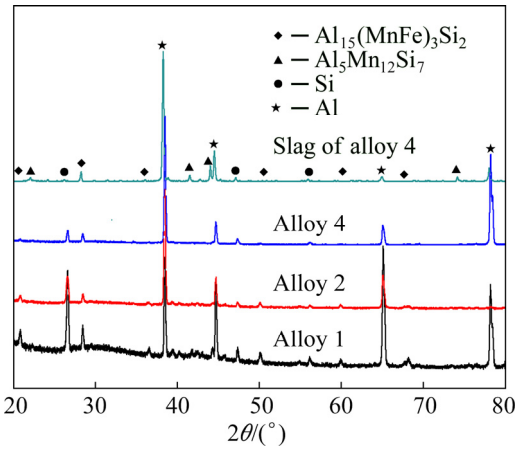

Fig. 8 XRD patterns of matrix and slag

and slag. In addition to the diffraction peaks of the Al and Si phases, a large number of iron-rich phase diffraction peaks were also found. The position difference in the diffraction peaks for different matrices is not obvious, but the peaks at 2θ of 20.821°, 50.080° and 59.950° in alloys 1 and 2 are significantly higher than those in alloy 4, which correspond to the $Al_{15}(MnFe)_3Si_2$ phase. Moreover, the peaks at 2θ of 22.098°, 42.777°, 44.520° in the slag of alloy 4 are significantly higher than those in the matrix, which is completely consistent with $Al_5Mn_{12}Si_7$.

Figure 9 presents the equilibrium phase distribution of Al−1.0Fe−Si−Mn at different temperatures. The results show that the equilibrium phases compositions of Al−7.0Si−1.0Fe−1.2Mn are ranked as follows: (1) liquid at 680−660 °C, (2) liquid and $Al_{15}Si_2M_4$ at 645−630 °C, (3) just lying in liquid, α(Al) and $Al_{15}Si_2M_4$ at 615 °C.

3.6 Mechanical properties

The tensile properties of the matrix are presented in Fig. 10. The tensile strength and elongation of the alloy gradually improved as the melt holding temperature decreased. When the holding temperature was 615 °C, the tensile strength and elongation of the matrix were increased by 11.6% and 82.8% compared to those holding at 680 °C, respectively, as well as slightly higher than those of the A356 alloy with a low Fe content [25].

Figure 11 presents images of cross-section fractures obtained at different holding temperatures. As shown in Fig. 11(a), the cracks originated from inner of the primary phases and propagated along the direction vertical to stretching. Subsequently, some microcracks were observed in the eutectic silicon phase and the Chinese script iron-rich phase. When the melt holding temperature was decreased to 630−660 °C, although the main fracture source was still the primary iron-rich phase, the expansion rate was less than that at 680 °C because a certain number of microcracks formed in the eutectic silicon and Chinese script iron-rich phases (Figs. 11(b) and (c)). When the melt holding temperature was 615 °C, cracks with a narrow shape were first observed in the eutectic silicon phase, and then some microcracks appeared in the Chinese script iron-rich phase (Fig. 11(d)). This result indicates that as the melt holding temperature

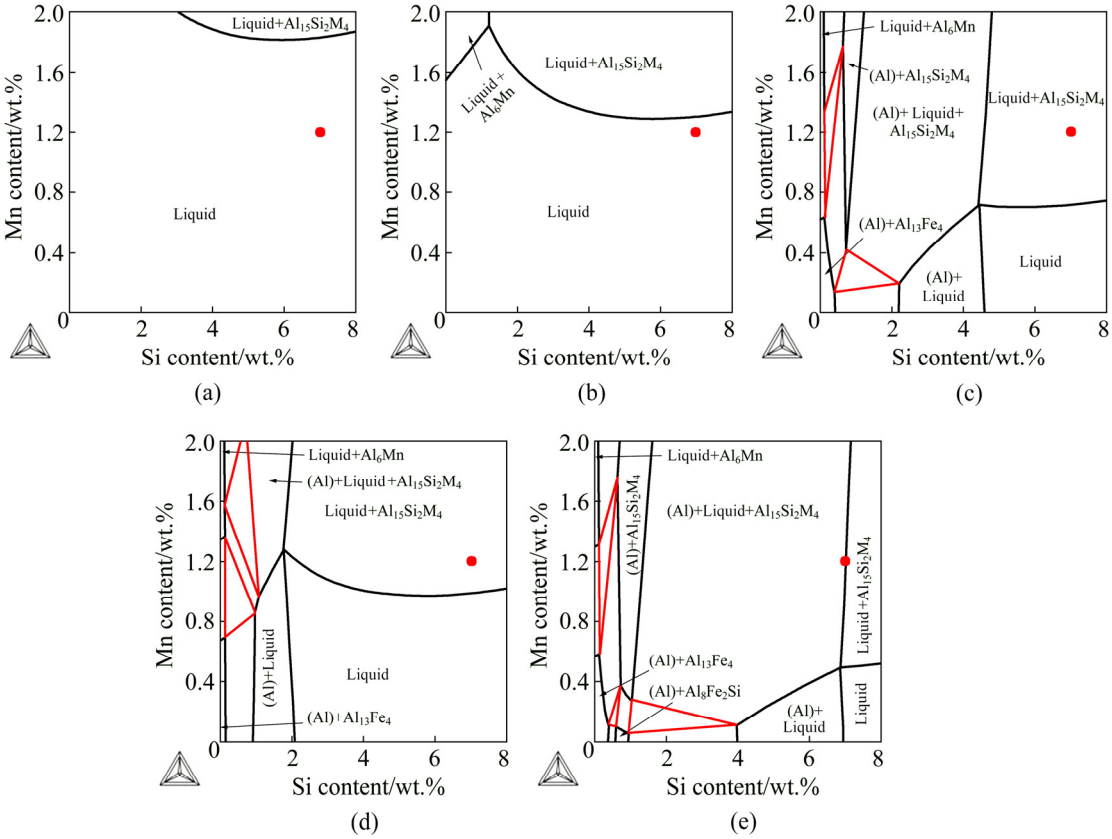

Fig. 9 Isothermal sections of Al−1.0Fe−Si−Mn alloys at different holding temperatures: (a) 680°C; (b) 660°C; (c) 645°C; (d) 630°C; (e) 615°C

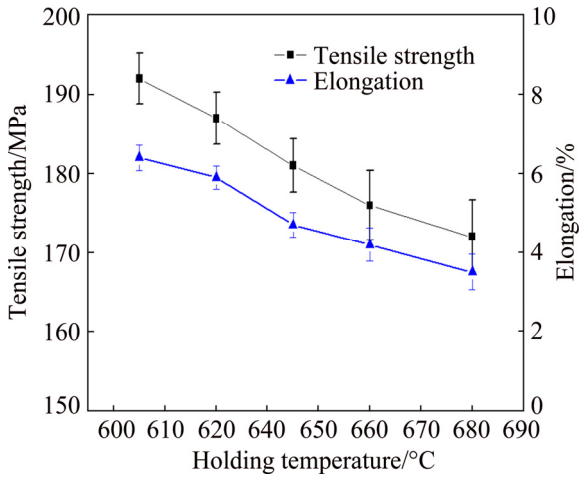

Fig. 10 Effects of holding temperature on mechanical properties of matrix

decreases, the main fracture origin changes from sludge to eutectic silicon, which significantly promotes the plasticity of the alloy.

4 Discussion

4.1 Evolution of mechanism underlying iron-rich phase morphology

Because Mn easily replaces Fe in the solid solution, adding Mn has become one of the most effective methods for improving the morphology of iron-rich phases and increasing the formation temperature of iron-rich phases [4]. The primary iron-rich phase is formed when the alloy contains certain contents of Fe, Mn, Cr and other elements, and the formation conditions are mainly determined by the alloy composition and cooling rate. To clarify how much Fe, Mn, and Cr is required for sludge formation, previous scholars [5] have usually used the sludge factor (SF, F_s) to judge the compositional conditions; its value can be calculated using the following empirical formula:

$$F_s=1w(\mathrm{Fe})+2w(\mathrm{Mn})+3w(\mathrm{Cr}) \quad (2)$$

Generally, the sludge phase might form when SF exceeds 1.70, but recent studies have shown that a primary iron-rich phase with a star-like morphology is observed even if the SF value is only 1.30−1.40 in the Al−12.7Si and AlSi9Cu3(Fe) alloys [5,19]. Furthermore, increasing the cooling rate is a beneficial method to suppress the slag phase formation when the SF value is between 1.47 and 1.76 [19]. In addition to the composition and cooling rate, the formation temperature also significantly affects the morphology, size and volume fraction of the slag phase. The higher the formation temperature is, the longer the growth

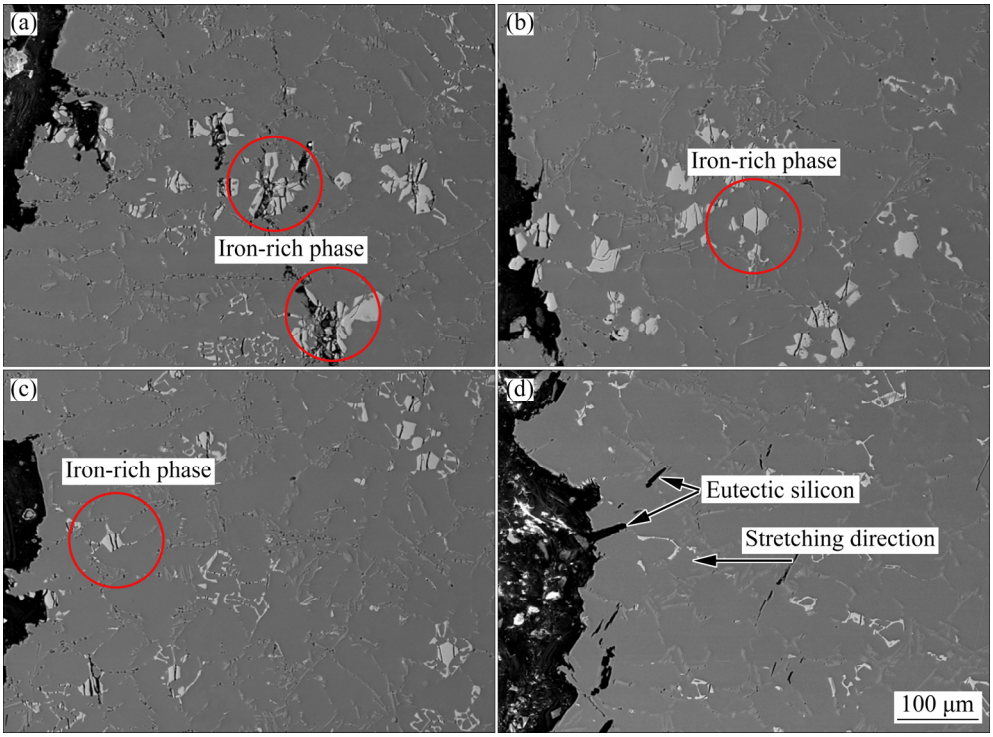

Fig. 11 Microstructures of tensile fracture sections obtained at different holding temperatures: (a) 680°C; (b) 660 °C; (c) 630 °C; (d) 615 °C

time and the bigger growth space, which leads to a larger size and volume fraction of the primary form. XU et al [26] used thermal analysis to study the effect of Mn/Fe mole ratio on the formation temperature of the sludge phase and found that the formation temperature is approximately 670−740 °C when n(Mn)/n(Fe)≥1.0 in Al−12%Si alloy. SHABESTARI and PARSHIZFARD [12] studied the effect of composition on the formation temperature of the sludge phase under rapid quenching and fitted a mathematical relationship between the formation temperature and Fe content [5]:

$$T=645.7+34.2\times w^2(\mathrm{Fe}) \quad (3)$$

Subsequently, TIMELLI et al [19] comprehensively considered the influence of Mn and Cr elements and the cooling rate on the formation temperature and fitted the relationship among the formation temperature, SF value and cooling rate for AlSi9Cu3(Fe) diecasting alloy:

$$T=34.7F_{\mathrm{S}}-0.82\frac{\mathrm{d}T}{\mathrm{d}t}+562 \quad (4)$$

The formation temperatures of the sludge phase as calculated using Eqs. (3) and (4) were 674.6 and 672.5 °C, respectively, which were slightly higher than the actual result of the DSC test (661.4 °C). Therefore, the evolution mechanism of the iron-rich phase morphology at different holding temperatures can be summarized as follows.

When melt holding was performed at 680 °C, the sludge phase could not nucleate and grow since the holding temperature was above the formation temperature. Upon casting at this temperature, sludge phases rapidly nucleated and grew under large undercooling conditions, and the growth direction was mainly controlled by the temperature gradient. Then, sludge phases with coarse sizes and star-like shapes were formed. As the sludge transforms, the contents of Mn and Fe gradually decrease until they fall below the composition condition of the primary phase, and then the transformations of the Chinese script rich-iron and α(Al) phases were started. Because the formation temperature partially overlapped with that of α(Al) [17], the two phases nucleated and grew completely, which led to the formation of slender Chinese script phases.

When the melt was held at 660 °C, the sludge phase nucleated and grew since the holding temperature was slightly below the formation temperature, but the growth rate was still low due to the small undercooling. A higher holding temperature was beneficial to the diffusion and migration of Mn and Fe atoms, which accelerated the sludge transformation to equiaxed crystals with the smallest free energy. A large number of sludge particles with fine size and a uniform distribution were formed, and the natural sedimentation was not significant. Upon casting after holding, the sludge phases grew rapidly based on these fine particles; the growth direction was mainly controlled by the temperature gradient. Then, sludge phases with polygonal connected to Chinese script and isolated Chinese script particles were formed.

When the melt temperature was decreased to 645−630 °C, the nucleation and growth rate of the sludge phase increased sharply with the greater undercooling, and the holding temperature guaranteed the fast diffusion of Mn and Fe. Therefore, a large amount of sludge phases with large size, high roundness and high density were formed during the holding process. For example, the average particle diameter of the primary phases was up to 55 μm at 630 °C, and the average roundness and Mn/Fe mole ratio were 1.16 and 1.7, respectively. Since the density of the sludge phases was 49.6% greater than that of the melt (2.34 g/cm^3), natural sedimentation of sludge occurred under gravity. With the consumption of Mn and Fe, the Mn/Fe mole ratio and density of the sludge formed at later stages gradually decreased, which was a result of the natural gravity sedimentation being blocked. These sludge phases remaining in the melt acted as nucleation cores and continued to grow. Eventually, low-density and irregular polygonal phases linked with Chinese script phases were found in the matrix. The remaining melt contained many minor sludge particles formed during holding, which acted as nucleation cores for the Chinese script, dense and short iron-rich phases. After holding at 615 °C, the SF of the residual melt was only 1.28, leading to no obvious sludge phases being observed.

In summary, the morphologies of primary iron-rich intermetallics in the matrix changed from star-like to polygonal, and then the mass of primary phases decreased gradually and disappeared at 615 °C, having instead a small, highly compact and evenly distributed Chinese script morphology.

4.2 Natural sedimentation control factors of sludge phase

The natural sedimentation of the sludge phase is a physical process, and the force and movement of sludge phases in the stratosphere melt can be analyzed using the Newton's second law. In addition to the gravity and buoyancy, the sludge is also affected by motion resistance (F_d), which can be calculated using the Stokes's formula as follows:

$$F_d=6\xi\pi rv \tag{5}$$

Furthermore, the force on the sludge can be expressed as follows:

$$F=4/3g\pi r^3(\rho_S-\rho_L)-6\xi\pi rv \tag{6}$$

where g is the gravitational acceleration; r is the equivalent radius; ρ_S is the density of the sludge; ρ_L is the density of the melt; ξ is the resistance coefficient, which is related to the surface friction caused by fluid viscosity; and v is the sedimentation velocity. According to the analysis of the formula, $F>0$ when v is small, and the sludge particles exhibit a vertical downward acceleration. Subsequently, F_d increases with increasing sedimentation velocity, while the acceleration gradually decreases. Finally, the force on the sludge is balanced, and the sludge phases move vertically downwards at a uniform speed. Therefore, the sedimentation velocity can be transformed to the following expression:

$$v=\frac{2}{9\xi}gr^2(\rho_S-\rho_L) \tag{7}$$

An analysis of formula (7) reveals that the natural sedimentation velocity of the primary iron-rich phase depends on the density difference between the sludge and melt, the equivalent radius of the sludge, and the resistance coefficient related to the fluid viscosity. Therefore, the sedimentation velocity is increased with increased density difference and sludge diameter as well as decreased resistance coefficient. However, ξ in formula (7) is related to the shape factor of the sludge phases. The closer the shape is to spherical, the smaller the resistance coefficient is. Therefore, the order of the sedimentation velocity of the sludge phases from large to small is regular polygonal, irregular polygonal and star-like. With decreasing temperature, the control factors of the natural sedimentation efficiency can be classified into three stages as follows.

In the first stage, when the holding temperature was 680 °C or above, the equivalent radius reached 30 μm, but the sludge was still unable to settle effectively due to the irregular morphology and density.

In the second stage, when the holding temperature was 660 °C, polygonal sludge with higher density formed, but the sedimentation efficiency was controlled by the radius.

In the third stage, when the holding temperature decreased to 630−645 °C, some of the sludge phases settled, while the others formed in later stages were unable to separate due to the lower density.

5 Conclusions

(1) With decreasing holding temperature, the sludge morphology in the matrix changed from star-like to polygonal, and then the mass of primary phases decreased gradually and disappeared at 615 °C, having instead a Chinese script with small size, high compact and uniform distribution. In contrast, the primary iron-rich phases in slag transformed to a coarser polygonal shape with lower roundness, and some of them had hollow structures. The (MnFe)/Si mole ratio of iron-rich intermetallics was mainly determined by their morphologies, while the substitution degree of Mn for Fe in intermetallics mainly depended on the holding temperature.

(2) With decreasing holding temperature, the area fraction of intermetallics and Fe content in matrix decreased gradually due to the formation and growth of sludge and subsequent natural sedimentation during melt holding. When the holding temperature was 615 °C, the concentrations of Fe and Mn in the matrix were 0.43% and 0.42%, respectively, which were 53.3% and 64.1% lower than those at 680 °C.

(3) The control factors of the iron-rich phase sedimentation efficiency with the holding temperature decreasing can be classified into three stages: morphology, size and density of sludge.

(4) With decreasing holding temperature, the tensile strength and elongation of the matrix gradually were improved by 11.6% and 82.8%, respectively. Meanwhile, the main fracture origin changed from sludge to eutectic silicon, which significantly promoted the plasticity of the alloy.

References

[1] DINNIS C M, TAYLOR J A, DAHLE A K. As-cast morphology of iron-intermetallics in Al−Si foundry alloys [J]. Scripta Materialia, 2005, 53(8): 955−958.

[2] TAYLOR J A. Iron-containing intermetallic phases in Al−Si based casting alloys [J]. Procedia Materials Science, 2012, 1: 19−33.

[3] ABOUEI V, SHABESTARI S G, SAGHAFUAN H. Dry sliding wear behaviour of hypereutectic Al−Si piston alloys containing iron-rich intermetallics [J]. Materials Characterization, 2010, 61(11): 1089−1096.

[4] JI S, YANG W, GAO F, WASTON D, FAN Z. Effect of iron on the microstructure and mechanical property of Al−Mg−Si−Mn and Al−Mg−Si diecast alloys [J]. Materials Science and Engineering A, 2013, 564(3):130−139.

[5] SHABESTARI S G. The effect of iron and manganese on the formation of intermetallic compounds in aluminum–silicon alloys [J]. Materials Science and Engineering A, 2004, 383(2): 289−298.

[6] FERRARO S, FABRIZI A, TIMELLI G. Evolution of sludge particles in secondary die-cast aluminum alloys as function of Fe, Mn and Cr contents[J]. Materials Chemistry & Physics, 2015, 153: 168−179.

[7] TZENG Y C, WU C T, BOR H Y, HORNG J L,TSAI M L,LEE S L. Effects of scandium addition on iron-bearing phases and tensile properties of Al−7Si−0.6Mg alloys [J]. Materials Science and Engineering A, 2014, 593: 103−110.

[8] KUMARI S S S, PILLAI R M, RAJAN T P D, PAI B C. Effects of individual and combined additions of Be, Mn, Ca and Sr on the solidification behaviour, structure and mechanical properties of Al−7Si−0.3Mg−0.8Fe alloy [J]. Materials Science and Engineering A, 2007, 460: 561−573.

[9] FAN Chao, LONG Si-yuan, WU Ming-fang, YANG Huai-de. Effect of Ce-rich mischmetal addition on microstructure and tensile properties of secondary Al−Si Alloys [J]. Rare Metal Materials and Engineering, 2014, 43(12): 3073−3077.

[10] TAN Xi-ping, ZHENG Kai-hong, SONG Dong-fu, ZHANG Xin-ming. Effects of A1−3B master alloy addition on impurity iron content of recycled casting aluminum alloy [J]. The Chinese Journal of Nonferrous Metals, 2014, 24(6): 1401−1407. (in Chinese)

[11] SEIFEDDINE S, JOHANSSON S, SVENSSON I L. The influence of cooling rate and manganese content on the β-Al_5FeSi phase formation and mechanical properties of Al−Si-based alloys [J]. Materials Science and Engineering A, 2008, 490(1−2): 385−390.

[12] SHABESTARI S G, PARSHIZFARD E. Effect of semi-solid forming on the microstructure and mechanical properties of the iron containing Al−Si alloys [J]. Journal of Alloys and Compounds, 2011, 509(30): 7973−7978.

[13] LIN Chong, WU Shu-sen, LÜ Shu-lin, WU He-bao, CHEN Han-xin. Influence of high pressure and manganese addition on Fe-rich phases and mechanical properties of hypereutectic Al−Si alloy with rheo-squeeze casting [J]. Transactions of Nonferrous Metals Society of China, 2019, 29(2): 253−262.

[14] CESCHINI L, BOROMEI I, MORRI A, SEIFEDDINE S, SVEBSSON I L. Microstructure, tensile and fatigue properties of the Al−10%Si−2%Cu alloy with different Fe and Mn content cast under controlled conditions [J]. Journal of Materials Processing Technology, 2009, 209(15−16): 5669−5679.

[15] HWANG J Y, DOTY H W, KAUFMAN M J. The effects of Mn additions on the microstructure and mechanical properties of Al−Si−Cu casting alloys [J]. Materials Science and Engineering A, 2008, 488(1−2): 496−504.

[16] SONG Dong-fu, WANG Shun-cheng, ZHENG Kai-hong. Effects of Mn/Fe mole ratio on iron-rich phase morphology of A356 cast aluminum alloy [J]. The Chinese Journal of Nonferrous Metals, 2015, 25(7): 1832−1838. (in Chinese)

[17] LOPES D M H, ROBERTO D O J, ROMANO E D C, SOARES T J A. Removal of iron from molten recycled aluminum through intermediate phase filtration [J]. Materials Transactions, 2006, 47(7): 1731−1736.

[18] LI Tian-xiao, XU Zhen-ming, SUN Bao-de, SHU Da, ZHOU Yao-he. Electromagnetic separation of primary iron-rich phases from aluminum-silicon melt [J]. Transactions of Nonferrous Metals Society of China, 2003, 13(1): 121−125.

[19] TIMELLI G, CAPUZZI S, FABRIZI A. Precipitation of primary Fe-rich compounds in secondary AlSi9Cu3(Fe) alloys [J]. Journal of Thermal Analysis and Calorimetry, 2015, 123(1): 249−262.

[20] ZHANG Lei, JIAO Wan-li, YU Hai-jun, YAO Guang-chun. Influence of manganese and pre-heat treatment on microstructure and mechanical properties of Al−Si alloy [J]. The Chinese Journal of Nonferrous Metals, 2005, 15(3): 368−373. (in Chinese)

[21] WANG Yao-wu, FENG Nai-xiang, SUN Ting, YOU Jing, QIN Jian. Mechanism of removing iron phase in Al−Si alloy by natural deposition [J]. Chinese Journal of Rare Metals, 2010, 34(1): 28−33. (in Chinese)

[22] CAO X, CAMPBELL J. The solidification characteristics of Fe-rich intermetallics in Al−11.5Si−0.4Mg cast alloys [J]. Metallurgical and Materials Transactions A, 2004, 35(5): 1425−1435.

[23] CHEN H L, CHEN Q, DU Y , BRATBERG J, ENGSTRÖM A . Update of Al−Fe−Si, Al−Mn−Si and Al−Fe−Mn−Si thermodynamic descriptions [J]. Transactions of Nonferrous Metals Society of China, 2014, 24(7): 2041−2053.

[24] FABRIZI A, TIMELLI G. The influence of cooling rate and Fe/Cr content on the evolution of Fe-rich compounds in a secondary Al−Si−Cu diecasting alloy[C]// International Conference on Advances in Solidification Processes. Windsor, UK: Iop Publishing Ltd., 2016: 12−17.

[25] LI Xiao-yan Y, LU Ya-lin, WANG Jian, ZHOU Dong-shuai, YANG Lin. Effect of rare earth Erbium on microstructure and mechanical properties of A356 aluminum alloy [J]. Journal of Materials Engineering, 2018, 46(1): 67−73.

[26] XU Z M, LI T X, ZHOU Y H. Elimination of Fe in Al−Si cast alloy scrap by electromagnetic filtration [J]. Journal of Materials Science, 2003, 38(22): 4557−4565.

熔体保温对 Al−Si−Fe−Mn−Mg 合金中富铁相形貌演变及其沉降行为的影响

宋东福[1,2]，王顺成[2]，赵愈亮[3]，刘树红[4]，杜 勇[4]，康跃华[2]，王 智[1]，张卫文[1]

1. 华南理工大学 国家金属材料近净成形工程技术研究中心，广州 510641；
2. 广东省材料与加工研究所，广州 510650；
3. 东莞理工学院 机械工程学院，东莞 523808；
4. 中南大学 粉末冶金国家重点实验室，长沙 410083

摘 要：采用光学显微镜、扫描电子显微镜、差热分析仪等研究保温温度对 Al−7.0Si−1.0Fe−1.2Mn−0.25Mg 合金中富铁相的形貌演变规律及沉降行为的影响。研究结果表明：随着熔体保温温度的降低，基体中初生富铁相形貌由星形向多边形转变，其数量逐渐减少并在 615 °C 时基本消失，形成细小、高致密且均匀分布的汉字状富铁相。而炉渣中的富铁相则向尺寸更为粗大、但圆整度更小的多边形转变，其中部分多边形为镂空结构。随保温温度的降低，基体中富铁相的面积分数及 Fe 含量逐渐降低，这是由于富铁相在熔体保温过程中形核、长大并发生自然沉降导致的。随着熔体保温温度的降低，阻碍初生富铁相沉降的主要因素依次为形貌、尺寸和密度。

关键词：Al−Si 合金；熔体保温；富铁相；形貌演变；沉降行为

(Edited by Xiang-qun LI)